Frontiers of Information Technology & Electronic Engineering
www.jzus.zju.edu.cn; engineering.cae.cn; www.springerlink.com
ISSN 2095-9184 (print); ISSN 2095-9230 (online)
E-mail: jzus@zju.edu.cn

Optimal federated fusion of multiple maneuvering targets based on multi-Bernoulli filters*#

Yu XUE, Xi'an FENG‡

School of Marine Science and Technology, Northwestern Polytechnical University, Xi'an 710072, China

E-mail: 18829236362@163.com; fengxa@nwpu.edu.cn

Received July 17, 2024; Revision accepted Dec. 1, 2024; Crosschecked Mar. 21, 2025; Published online May 2, 2025

Abstract: A federated fusion algorithm of joint multi-Gaussian mixture multi-Bernoulli (JMGM-MB) filters is proposed to achieve optimal fusion tracking of multiple uncertain maneuvering targets in a hierarchical structure. The JMGM-MB filter achieves a higher level of accuracy than the multi-model Gaussian mixture MB (MM-GM-MB) filter by propagating the state density of each potential target in the interactive multi-model (IMM) filtering manner. Within the hierarchical structure, each sensor node performs a local JMGM-MB filter to capture survival, newborn, and vanishing targets. A notable characteristic of our algorithm is a master filter running on the fusion node, which can help identify the origins of state estimates and supplement missed detections. The outputs of all filters are associated into multiple groups of single-target estimates. We rigorously derive the optimal fusion of IMM filters and apply it to merge associated single-target estimates. This optimality is guaranteed by the covariance upper-bounding technique, which can truly eliminate correlations among filters. Simulation results demonstrate that the proposed algorithm outperforms the existing centralized and distributed fusion algorithms in linear and heterogeneous scenarios, and the relative weights of the master and local filters can be adjusted flexibly.

Key words: Uncertain maneuvering targets; Joint multi-Gaussian mixture multi-Bernoulli (JMGM-MB) filter; Hierarchical structure; Optimal fusion; Correlations

https://doi.org/10.1631/FITEE.2400598 **CLC number:** TP273.5

1 Introduction

Decentralized fusion tracking of multiple maneuvering targets aims to estimate multi-target states by integrating the outputs of multiple local filters. The soft decision problem of maneuvering targets' motion models is generally addressed by local filters (Zhao, 2024).

So far, the joint use of the jump Markov (JM) theory (Balenzuela et al., 2022) and the random finite set (RFS) filtering theory (Mahler, 2014) has been the most successful attempt at tracking multiple maneuvering targets. In the JM theory, multiple model-conditioned tracking filters are performed in parallel, and their filtering results are mutually interacted according to the Markovian chain to resolve the target dynamic model uncertainty. Inspired by the interactive multi-model (IMM) theory (Chang and Athans, 1978), the first genuine JM-RFS filter is the multi-model (MM) implementation of the probability hypothesis density (PHD) filter (Punithakumar et al., 2008), which propagates the first-order moment of the full multi-target density. An MM tracking system is constructed based on the cardinalized PHD (CPHD) filter that simultaneously propagates the multi-target PHD and its cardinality distribution (Georgescu and Willett, 2012). The multi-Bernoulli (MB) filter exhibits superiority over the PHD and CPHD filters in single-model

‡ Corresponding author

* Project supported by the National Natural Science Foundation of China (No. 62071386)

Electronic supplementary materials: The online version of this article (https://doi.org/10.1631/FITEE.2400598) contains supplementary materials, which are available to authorized users

ORCID: Yu XUE, https://orcid.org/0000-0002-7177-5140

scenarios (Vo et al., 2009; Yi et al., 2020; Hu XL et al., 2022) since it gets closer to the full multi-target density. The work that is most representative of the MM-MB filter (Dunne and Kirubarajan, 2013; Xie XX et al., 2023) models the state probability density function (PDF) as a function of the state and model variables. Of course, there are some other implementations of the JM-RFS filter (Li WL and Jia, 2011; Wu WH et al., 2021a), such as the straightforward fitting of the dynamical state evolution matrix and the MM-labeled MB (MM-LMB) filter. An alternative to the MB-based MM filter (Wu SY et al., 2019) assigns a model probability vector to the estimate of each potential target. This vector will absorb the differences in measurement likelihoods under different models and favor the true model in combining model-conditioned estimates of the same target. Every MM-RFS filter can be implemented using the Gaussian mixture (GM) method (Dong et al., 2021; Sun YC et al., 2022) and the sequential Monte Carlo (SMC) method (Ouyang et al., 2012; Zhou et al., 2024). We proposed a joint multi-Gaussian mixture multi-Bernoulli (JMGM-MB) filter that outperforms the MM-GM-MB filter in both active and passive tracking scenarios (Xue and Feng, 2024). In this filter, each potential maneuvering target's state estimate is characterized by a set of parallel model-related Gaussian functions with model probabilities, and a weight quantifies the possibility of this estimate. These model-related parameters are propagated in the full IMM filtering manner and thus can capture unknown target maneuvers adaptively. The JMGM-MB filter maintains the single-model MB filtering form, resulting in more friendly computation than the MM-GM-MB filter.

In decentralized density fusion of MM-RFS filters, the locally filtered cardinality and state estimates rather than the model uncertainty are the fusion methods' interest, given that the fusion methods may use but never change the model labels of locally filtered estimates, if any. A typical density fusion scheme is to generalize the single-target covariance intersection (CI) fusion (Julier and Uhlmann, 1997) to multi-target scenarios (Üney et al., 2013; Gunay et al., 2016), which is also known as geometric average (GA) fusion as each local density is allotted an exponential weight. In other works (Xie X et al., 2019; Wu WH et al., 2021b), local filters provide outputs independent of the model. A more reliable GA fusion involves fusing outputs with the same model label (Li GY et al., 2024). However, GA fusion tends to underestimate the target number, especially in scenarios involving multiple sensor nodes (Üney et al., 2019), and it behaves poorly when missed detections occur frequently or the target trajectories intersect (Gao et al., 2020). In recent years, the mainstream version of density fusion is arithmetic average (AA) fusion, which integrates locally filtered densities by weighted sum (Li TC et al., 2020, 2024b; Wang et al., 2024). Although computationally concise, AA fusion can yield better performance than GA fusion in tracking accuracy and tolerance to missed detections (Li TC et al., 2019b; Li TC, 2024; Shen-Tu et al., 2024). An important reason for this superiority is that AA fusion employs association to decompose multi-target fusion into multiple single-target fusions, avoiding the mutual interference of different targets. In some research (Da et al., 2020a; Peng et al., 2021), local filter outputs with the same model label are integrated in the AA manner. Additionally, AA fusion can be realized in diverse forms, like a hierarchical structure (Yang et al., 2024). Both AA and GA fusion can obtain the minimum sum of Kullback–Leibler divergences of local densities (Da et al., 2020b) and the Fréchet mean.

So far, no fusion approach has been applied to integrate the JMGM-MB filters mentioned above. The AA fusion scheme can be easily extended to realize this. However, an inevitable problem is the ubiquitous correlations arising from common target process noise and feedback (Sun SL, 2020). It is impractical to record and handle these correlations in the presence of random false alarms, missed detections, and target new births. The existing AA fusion methods cannot adopt better decorrelation merging means than the CI or covariance union (CU) method (Wei et al., 2023; Li TC et al., 2024a). Since the two merging methods fail to truly eliminate the correlations involved, the AA fusion algorithms are suboptimal. Decorrelation is always challenging for AA fusion.

This paper proposes the optimal federated fusion of JMGM-MB filters to achieve optimal decentralized fusion tracking of a time-varying number of maneuvering targets. The major contributions include:

1. Derive the optimal fusion of single-target IMM filters, during which the covariance upper-bounding technique is introduced to truly eliminate correlations.

2. Decompose multi-target fusion into multiple single-target fusions by association. The derived optimal single-target fusion requires a master filter to record prior density and supplement missed detections. Hence, our algorithm features a hierarchical structure.

3. Realize the centralized product multi-sensor (PM) fusion and decentralized AA fusion of JMGM-MB filters, which have not yet been investigated.

2 Preliminaries for the JMGM-MB filter

In a network involving S sensor nodes, let $\boldsymbol{Z}_{1:k}^{(s)}$ denote the s^{th} sensor's measurements cumulated until time k. The multi-target density of filter s at time k is

$$p\left(\boldsymbol{X}|\boldsymbol{Z}_{1:k}^{(s)}\right)=\pi_k^{(s)}=\left\{\left(r_k^{(s,v)},p_k^{(s,v)}\right)\right\}_{v=1}^{M_k^{(s)}}, \tag{1}$$

where $\boldsymbol{X}$ is a variable of multi-target state RFS, $p_k^{(s,v)}$ is the state PDF of a potential target characterized by an existence probability $r_k^{(s,v)}$, and $M_k^{(s)}$ is the number of potential targets. Hereinafter, (r,p) is collectively called a Bernoulli component (BC).

We derive a JMGM model to implement the MB filter (Xue and Feng, 2024), where the state PDF $p_k^{(s,v)}$ is expressed as

$$p_k^{(s,v)}=\sum_{i=1}^{J_k^{(s,v)}}\omega_{k,i}^{(s,v)}\sum_{m=1}^{N}u_{k,i,m}^{(s,v)}\mathcal{N}\left(\boldsymbol{x};\boldsymbol{m}_{k,i,m}^{(s,v)},\boldsymbol{P}_{k,i,m}^{(s,v)}\right), \tag{2}$$

where $\sum_{m=1}^{N}u_{k,i,m}^{(s,v)}\mathcal{N}(\boldsymbol{x};\boldsymbol{m}_{k,i,m}^{(s,v)},\boldsymbol{P}_{k,i,m}^{(s,v)})$ is a PDF hypothesis which assumes that the v^{th} potential target's motion is governed by the m^{th} model with a probability of $u_{k,i,m}^{(s,v)}\left(\sum_{m=1}^{N}u_{k,i,m}^{(s,v)}=1\right)$. In addition, $\boldsymbol{m}_{k,i,m}^{(s,v)}$ and $\boldsymbol{P}_{k,i,m}^{(s,v)}$ are the model-conditioned state estimate and error covariance, respectively, N is the number of possible models, $\omega_{k,i}^{(s,v)}$ is this PDF hypothesis's possibility/weight, and $J_k^{(s,v)}$ is the number of PDF hypotheses. Hereinafter, $\left(\omega,(u_m,\boldsymbol{m}_m,\boldsymbol{P}_m)_{m=1}^{N}\right)$ is called a JMGM component and serves as the smallest data unit in the JMGM-MB filter.

The model-conditioned $(u_m,\boldsymbol{m}_m,\boldsymbol{P}_m)_{m=1}^{N}$ is propagated in the full IMM manner, including interaction, prediction, and updating, so each JMGM component can be regarded as a weighted IMM filter. The components of newborn targets do not need the former two operations as they are generated at the current time k. Clearly, fusing multiple JMGM-MB filters involves fusing multiple IMM filters.

3 Optimal fusion of a single maneuvering target

This section derives the optimal fusion of IMM filters in the absence and presence of missed detections, which will be used in Section 4 to merge JMGM components.

3.1 In the absence of missed detections

Suppose S linear sensors are tracking a maneuvering target with state $\boldsymbol{x}$, and the sensor with index s (s=1, 2, ⋯, S) acquires its measurement $\boldsymbol{z}^{(s)}$ using linear observation model $\boldsymbol{z}^{(s)}=\boldsymbol{H}^{(s)}\boldsymbol{x}+\boldsymbol{v}^{(s)}$, where $\boldsymbol{H}^{(s)}$ is the observation matrix and $\boldsymbol{v}^{(s)}$ is the Gaussian observation noise with covariance $\boldsymbol{R}^{(s)}$. The observation noises of these sensor nodes are independent. Assume that the prior state density of the maneuvering target above can be expressed as the following IMM form:

$$p(\boldsymbol{x})=\sum_{m=1}^{N}u_m p_m(\boldsymbol{x})=\sum_{m=1}^{N}u_m\mathcal{N}(\boldsymbol{x};\boldsymbol{m}_m,\boldsymbol{P}_m), \tag{3}$$

where $p_m(\boldsymbol{x})=\mathcal{N}(\boldsymbol{x};\boldsymbol{m}_m,\boldsymbol{P}_m)$ is the prior density under the m^{th} model with model-conditioned probability u_m, mean $\boldsymbol{m}_m$, and covariance $\boldsymbol{P}_m$.

Let $p(\boldsymbol{x}|\boldsymbol{Z})=\sum_{m=1}^{N}u_m(\boldsymbol{Z})\,p_m(\boldsymbol{x}|\boldsymbol{Z})=\sum_{m=1}^{N}u_m(\boldsymbol{Z})\cdot\mathcal{N}(\boldsymbol{x};\boldsymbol{m}_m(\boldsymbol{Z}),\boldsymbol{P}_m(\boldsymbol{Z}))$ denote the posterior state density with model-conditioned posterior estimate $\boldsymbol{m}_m(\boldsymbol{Z})$, error covariance $\boldsymbol{P}_m(\boldsymbol{Z})$, and probability $u_m(\boldsymbol{Z})$, $\boldsymbol{Z}=\bigcup_{s=1}^{S}\{\boldsymbol{z}^{(s)}\}$. According to the Bayesian rule, the following two equations hold:

$$\begin{aligned}p_m(\boldsymbol{x}|\boldsymbol{Z})&=\mathcal{N}\left(\boldsymbol{x};\boldsymbol{m}_m(\boldsymbol{Z}),\boldsymbol{P}(\boldsymbol{Z})\right)\\&=\frac{\prod_{s=1}^{S}g\left(\boldsymbol{z}^{(s)}|\boldsymbol{x},m\right)\mathcal{N}\left(\boldsymbol{x};\boldsymbol{m}_m,\boldsymbol{P}_m\right)}{\int\prod_{s=1}^{S}g\left(\boldsymbol{z}^{(s)}|\boldsymbol{x},m\right)\mathcal{N}\left(\boldsymbol{x};\boldsymbol{m}_m,\boldsymbol{P}_m\right)\mathrm{d}\boldsymbol{x}},\end{aligned} \tag{4}$$

$$u_m(\boldsymbol{Z})=\frac{\prod_{s=1}^{S} g_m\left(\boldsymbol{z}^{(s)}\right)\cdot u_m}{\sum_{m=1}^{N}\prod_{s=1}^{S} g_m\left(\boldsymbol{z}^{(s)}\right)\cdot u_m}, \tag{5}$$

where $g(\boldsymbol{z}^{(s)}|\boldsymbol{x}, m)$ is the likelihood function of $\boldsymbol{z}^{(s)}$ under the m^{th} model, and the likelihood $g_m(\boldsymbol{z}^{(s)})=\int g(\boldsymbol{z}^{(s)}|\boldsymbol{x}, m)\, p_m(\boldsymbol{x})\mathrm{d}\boldsymbol{x}$. Given the linear observation model above, $g(\boldsymbol{z}^{(s)}|\boldsymbol{x}, m)=\mathcal{N}(\boldsymbol{z}^{(s)}|\boldsymbol{H}^{(s)}\boldsymbol{x}, \boldsymbol{R}^{(s)})$, which is actually independent of the model. Applying it to Eq. (4) and $g_m(\boldsymbol{z}^{(s)})$, we can obtain

$$\boldsymbol{P}_m^{-1}(\boldsymbol{Z})\boldsymbol{m}_m(\boldsymbol{Z})=\boldsymbol{P}_m^{-1}\boldsymbol{m}_m+\sum_{s=1}^{S}\left(\boldsymbol{H}^{(s)}\right)^{\mathrm{T}}\left(\boldsymbol{R}^{(s)}\right)^{-1}\boldsymbol{z}^{(s)}, \tag{6}$$

$$\boldsymbol{P}_m^{-1}(\boldsymbol{Z})=\boldsymbol{P}_m^{-1}+\sum_{s=1}^{S}\left(\boldsymbol{H}^{(s)}\right)^{\mathrm{T}}\left(\boldsymbol{R}^{(s)}\right)^{-1}\boldsymbol{H}^{(s)}, \tag{7}$$

$$g_m\left(\boldsymbol{z}^{(s)}\right)=\mathcal{N}\left(\boldsymbol{z}^{(s)}|\boldsymbol{H}^{(s)}\boldsymbol{m}_m, \boldsymbol{H}^{(s)}\boldsymbol{P}_m\left(\boldsymbol{H}^{(s)}\right)^{\mathrm{T}}+\boldsymbol{R}^{(s)}\right). \tag{8}$$

As we can see, computing the posterior state density $p(\boldsymbol{x}|\boldsymbol{Z})$ requires all sensor measurements $\boldsymbol{Z}$, which may incur a considerable communication burden. Hence, we reshape Eqs. (6), (7), and (5) as

$$\boldsymbol{P}_m^{-1}(\boldsymbol{Z})\boldsymbol{m}_m(\boldsymbol{Z})=\beta(0)\boldsymbol{P}_m^{-1}\boldsymbol{m}_m+\sum_{s=1}^{S}\beta(s)\boldsymbol{P}_m^{-1}\boldsymbol{m}_m+\left(\boldsymbol{H}^{(s)}\right)^{\mathrm{T}}\left(\boldsymbol{R}^{(s)}\right)^{-1}\boldsymbol{z}^{(s)}, \tag{9}$$

$$\boldsymbol{P}_m^{-1}(\boldsymbol{Z})=\beta(0)\boldsymbol{P}_m^{-1}+\sum_{s=1}^{S}\beta(s)\boldsymbol{P}_m^{-1}+\left(\boldsymbol{H}^{(s)}\right)^{\mathrm{T}}\left(\boldsymbol{R}^{(s)}\right)^{-1}\boldsymbol{H}^{(s)}, \tag{10}$$

$$u_m(\boldsymbol{Z})=\frac{u_m\cdot\prod_{s=1}^{S}\left(g_m\left(\boldsymbol{z}^{(s)}\right)u_m\right)/u_m^{S}}{\sum_{m=1}^{N}u_m\cdot\prod_{s=1}^{S}\left(g_m\left(\boldsymbol{z}^{(s)}\right)u_m\right)/u_m^{S}}, \tag{11}$$

where $\beta(s)$ (s=0, 1, ⋯, S) represents a group of positive average factors, $\sum_{s=0}^{S}\beta(s)=1$.

Let $\boldsymbol{m}_m^{(s)}=\boldsymbol{P}_m^{(s)}[\beta(s)\boldsymbol{P}_m^{-1}\boldsymbol{m}_m+(\boldsymbol{H}^{(s)})^{\mathrm{T}}(\boldsymbol{R}^{(s)})^{-1}\cdot\boldsymbol{z}^{(s)}]$ with $\boldsymbol{P}_m^{(s)}=[\beta(s)\boldsymbol{P}_m^{-1}+(\boldsymbol{H}^{(s)})^{\mathrm{T}}(\boldsymbol{R}^{(s)})^{-1}\cdot\boldsymbol{H}^{(s)}]^{-1}$ and $u_m^{(s)}=g_m(\boldsymbol{z}^{(s)})u_m\Big/\sum_{m=1}^{N}g_m(\boldsymbol{z}^{(s)})u_m$. Then $p(\boldsymbol{x}\,|\,\boldsymbol{z}^{(s)})=\sum_{m=1}^{N}u_m^{(s)}\mathcal{N}(\boldsymbol{x};\boldsymbol{m}_m^{(s)}, \boldsymbol{P}_m^{(s)})$ is an IMM filter using $\sum_{m=1}^{N}u_m\mathcal{N}(\boldsymbol{x};\boldsymbol{m}_m, 1/\beta(s)\boldsymbol{P}_m)$ and $\boldsymbol{z}^{(s)}$ as the prior state density (s=1, 2, ⋯, S). Let $\boldsymbol{m}_m^{(0)}=\boldsymbol{m}_m$, $\boldsymbol{P}_m^{(0)}=1/\beta(0)\boldsymbol{P}_m$, and $u_m^{(0)}=u_m$. Then an extra facility is required to record $\sum_{m=1}^{N}u_m^{(0)}\mathcal{N}(\boldsymbol{x};\boldsymbol{m}_m^{(0)}, \boldsymbol{P}_m^{(0)})$.

Then, the model-conditioned means, covariances, and probabilities of the posterior state PDF $p(\boldsymbol{x}|\boldsymbol{Z})$ become

$$\boldsymbol{P}_m^{-1}(\boldsymbol{Z})\boldsymbol{m}_m(\boldsymbol{Z})=\sum_{s=0}^{S}\left(\boldsymbol{P}_m^{(s)}\right)^{-1}\boldsymbol{m}_m^{(s)}, \tag{12}$$

$$\boldsymbol{P}_m^{-1}(\boldsymbol{Z})=\sum_{s=0}^{S}\left(\boldsymbol{P}_m^{(s)}\right)^{-1}, \tag{13}$$

$$u_m(\boldsymbol{Z})=\frac{\prod_{s=0}^{S}u_m^{(s)}\Big/\left(u_m^{(0)}\right)^{S}}{\sum_{m=1}^{N}\prod_{s=0}^{S}u_m^{(s)}\Big/\left(u_m^{(0)}\right)^{S}}. \tag{14}$$

As we can see, after assigning the expanded prior covariances $1/\beta(s)\boldsymbol{P}_m$ (m=1, 2, ⋯, N) to different IMM filters (s=1, 2, ⋯, S) and an extra facility (s=0), the means and error covariances in the naïve covariance convex (CC) fusion form, as given in Eqs. (12) and (13), and the model probabilities in product form, as given in Eq. (14), are equivalent to the optimal Bayesian fusion in Eqs. (4)–(8).

The optimality above can also be proven by the covariance upper-bounding technique (Carlson, 1990). The content of this technique is provided in the supplementary materials.

3.2 In the presence of missed detections

If one sensor with index s misses the target state $\boldsymbol{x}$, i.e., $\boldsymbol{z}^{(s)}=\varnothing$, then the Bayesian fusion in Eqs. (4) and (5) will adopt $g(\varnothing|\boldsymbol{x}, m)=1/\mathbb{X}$ and $g_m(\varnothing)=1$ with the state space $\mathbb{X}$, which means that no model is supported due to the lack of measurements. Meanwhile, Eqs. (6), (7), (9), and (10) will take out $(\boldsymbol{H}^{(s)})^{\mathrm{T}}(\boldsymbol{R}^{(s)})^{-1}\boldsymbol{z}^{(s)}$ and $(\boldsymbol{H}^{(s)})^{\mathrm{T}}(\boldsymbol{R}^{(s)})^{-1}\boldsymbol{H}^{(s)}$. To maintain the decentralized fusion structure involving S sensors, the model-conditioned estimates, covariances, and probabilities of sensor s in Eqs. (12)–(14) will be replaced by

$$\boldsymbol{m}_m^{(s)}=\boldsymbol{m}_m,\ \boldsymbol{P}_m^{(s)}=1/\beta(s)\,\boldsymbol{P}_m,\ u_m^{(s)}=u_m. \tag{15}$$

Fortunately, the facility with index $s=0$ can provide these data via

$$\boldsymbol{m}_m^{(s)}=\boldsymbol{m}_m^{(0)},\ \boldsymbol{P}_m^{(s)}=\beta(0)/\beta(s)\,\boldsymbol{P}_m^{(0)},\ u_m^{(s)}=u_m^{(0)}. \quad (16)$$

In conclusion, when sensor s encounters a missed detection, the decentralized fusion in Eqs. (12)–(14) is still optimal by supplementing the missed estimates, covariances, and model probabilities with the extra facility. This conclusion will hold even if more than one sensor encounters missed detections.

4 Optimal federated fusion of multiple maneuvering targets

This section proposes a federated fusion of JMGM-MB filters, which can eliminate correlations among filters.

4.1 Hierarchical fusion structure

Inspired by the optimal single-target fusion in Section 3, we design a hierarchical structure for the proposed fusion algorithm, as shown in Fig. 1. Sensor nodes use measurements to perform local JMGM-MB filters. A fusion node does not observe targets but is responsible for (1) a master JMGM-MB filter that performs only prediction, (2) collecting, associating, and merging the locally filtered multi-target densities, and (3) assigning the fusion result and some filter parameters to each filter.

In Fig. 1, circles represent BCs, while tricolor rectangles inside circles represent JMGM components $(\omega,(u_m,\boldsymbol{m}_m,\boldsymbol{P}_m)_{m=1}^{N})$. The fusion node collects several BCs with large existence probabilities and labels them with their filter indices. Association decomposes multi-target fusion into multiple single-target fusions. By virtue of filter index labels, the fusion node is able to judge the origination of associated BCs. Each origination employs a particular merging method for JMGM components. According to the covariance upper-bounding technique (Carlson, 1990), information assignment can eliminate correlations originating from feedback and common process noise. Local filters can identify target new births and target vanishing using sensor measurements, whereas the master filter solely propagates the fusion result of the previous time. The predicted fusion result is the prior density of the current time, and thus, the master filter serves as the facility mentioned in Section 3 to record the prior estimates.

4.2 Federated fusion of JMGM-MB filters

Suppose that the hierarchical structure above consists of S sensor nodes and one fusion node. Let $s=0$ represent the fusion node and its master filter,

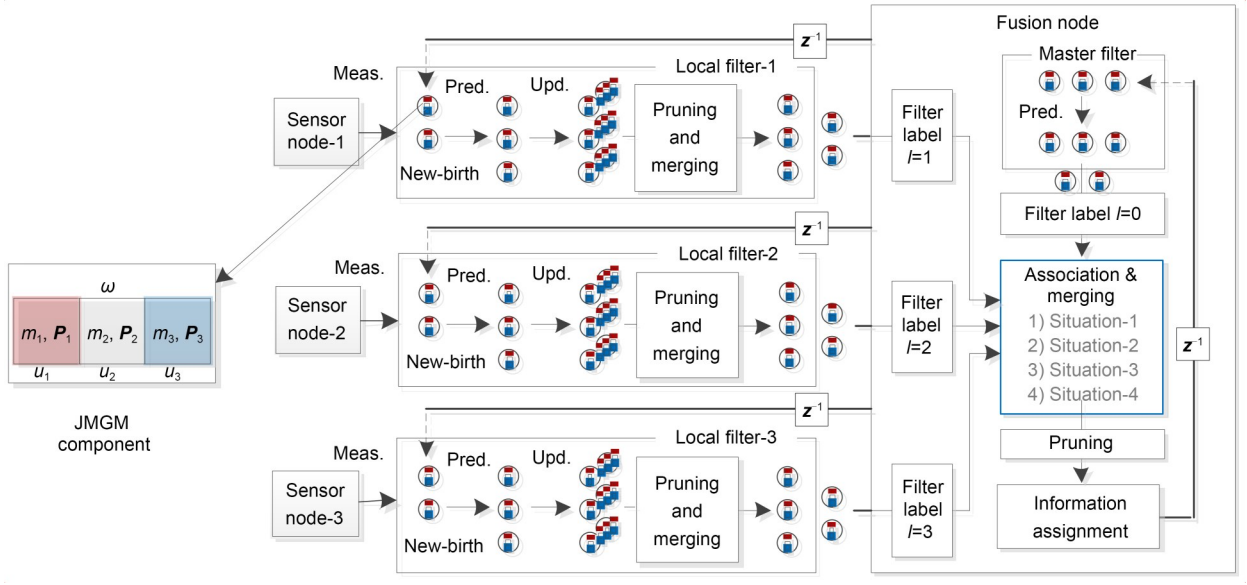

Fig. 1 Structure of the proposed federated fusion of JMGM-MB filters (assuming the number of models N=3). Meas.: measurement; Pred.: prediction; Upd.: update

and let $s=1, 2, \cdots, S$ represent the sensor nodes and their local filters. We prescribe that all sensor nodes share the same field of view.

1. Information assignment

Suppose that at time $k-1$, the multi-target density of each filter is $\pi_{k-1}^{(s)}=\{(r_{k-1}^{(s,v)}, p_{k-1}^{(s,v)})\}_{v=1}^{M_{k-1}^{(s)}}$, $s=0, 1, \cdots, S$, as stated in Eqs. (1) and (2). The fused density is

$$\pi_{k-1}^{(\mathrm{F})}=\{(r_{k-1}^{(\mathrm{F},v)}, p_{k-1}^{(\mathrm{F},v)})\}_{v=1}^{M_{k-1}^{(\mathrm{F})}}, \tag{17}$$

where $M_{k-1}^{(\mathrm{F})}$ is the number of fused BCs, and the v^{th} fused BC is characterized by an existence probability $r_{k-1}^{(\mathrm{F},v)}$ and a state PDF $p_{k-1}^{(\mathrm{F},v)}$ that can be expressed as the following JMGM form:

$$p_{k-1}^{(\mathrm{F},v)}=\sum_{i=1}^{J_{k-1}^{(\mathrm{F},v)}}\omega_{k-1,i}^{(\mathrm{F},v)}\sum_{m=1}^{N}u_{k-1,i,m}^{(\mathrm{F},v)}\mathcal{N}(\boldsymbol{x};\boldsymbol{m}_{k-1,i,m}^{(\mathrm{F},v)},\boldsymbol{P}_{k-1,i,m}^{(\mathrm{F},v)}), \tag{18}$$

with the number of JMGM components $J_{k-1}^{(\mathrm{F},v)}$ and the i^{th} JMGM component $(\omega_{k-1,i}^{(\mathrm{F},v)}, (u_{k-1,i,m}^{(\mathrm{F},v)}, \boldsymbol{m}_{k-1,i,m}^{(\mathrm{F},v)}, \boldsymbol{P}_{k-1,i,m}^{(\mathrm{F},v)})_{m=1}^{N})$.

For the optimal fusion of a single maneuvering target, as given in Eqs. (9)–(14), the crux is to assign the fused covariance to each filter using average factors. By doing so, the correlations among filters can be eliminated, thereby achieving the same optimal fusion accuracy as centralized fusion. Inspired by this, the fused density in Eqs. (17) and (18) and the process noise covariance are assigned to the master and local filters ($s=0, 1, \cdots, S$) via

$$\begin{aligned}\left\{r_{k-1}^{(s,v)}, p_{k-1}^{(s,v)}\right\}_{v\in\mathcal{S}_{k-1}^{(s)}}=&\left\{r_{k-1}^{(\mathrm{F},v)}, \sum_{i=1}^{J_{k-1}^{(\mathrm{F},v)}}\omega_{k-1,i}^{(\mathrm{F},v)}\right.\\ &\left.\cdot\sum_{m=1}^{N}u_{k-1,i,m}^{(\mathrm{F},v)}\mathcal{N}\left(\boldsymbol{x};\boldsymbol{m}_{k-1,i,m}^{(\mathrm{F},v)},\frac{1}{\beta(s)}\boldsymbol{P}_{k-1,i,m}^{(\mathrm{F},v)}\right)\right\}_{v=1}^{M_{k-1}^{(\mathrm{F})}},\end{aligned} \tag{19}$$

$$\boldsymbol{Q}_m^{(s)}=1/\beta(s)\,\boldsymbol{Q}_m,\quad m=1, 2, \cdots, N, \tag{20}$$

where $\mathcal{S}_{k-1}^{(s)}=\{v|\arg\max_v\sum r_{k-1}^{(s,v)}, |\mathcal{S}_{k-1}^{(s)}|=M_{k-1}^{(\mathrm{F})}\}$ represents the superscripts of $M_{k-1}^{(\mathrm{F})}$ BCs with the largest existence probabilities in filter s, $\beta(s)$ is the average factor of filter s, $\boldsymbol{Q}_m^{(s)}$ is the model-conditioned process noise covariance assigned to filter s with the full process noise covariance $\boldsymbol{Q}_m$, and "$\{\cdot,\cdot\}=\{\cdot,\cdot\}$" is used to assign values to BCs.

The correlations originating from feedback and common process noise are eliminated by Eqs. (19) and (20), respectively.

Since the covariances of JMGM components are increased by $(\beta(s))^{-1}$ times, their distances are reduced to $1/\beta(s)$ of their original values, and the merging threshold of filter s $\left(\lambda_{\mathrm{m}}^{(s)}\right)$ should be adjusted as

$$\lambda_{\mathrm{m}}^{(s)}=\beta(s)\lambda_{\mathrm{m}},\quad s=0, 1, \cdots, S, \tag{21}$$

with the full merging threshold λ_{m}.

2. Master and local filters

The JMGM-MB filter we proposed is used as the master and local filters.

First, the master and local filters predict their BCs using assigned process noise covariance $\boldsymbol{Q}_m^{(s)}$, during which every JMGM component is interacted and then predicted in the IMM manner. Each filter introduces newborn target BCs based on the same prior information. Then, the predicted multi-target densities are uniformly recorded as $\pi_{k|k-1}^{(s)}$ ($s=0, 1, \cdots, S$). The master filter uses the predicted density as its posterior density, i.e., $\pi_k^{(0)}=\pi_{k|k-1}^{(0)}$. Local filters use sensor measurements to modify their predicted multi-target densities/existence probabilities and JMGM components, including compensation for missed detections and updating using measurements. The BCs with existence probabilities smaller than $\lambda_{\mathrm{d}}^{\mathrm{BC}}$ and the JMGM component with weights smaller than $\lambda_{\mathrm{d}}^{\mathrm{JMGM}}$ are directly discarded. The JMGM components with distances smaller than $\lambda_{\mathrm{m}}^{(s)}$ are merged into one. In the end, the posterior multi-target densities of the master and local filters are uniformly recorded as $\pi_k^{(s)}=\left\{\left(r_k^{(s,v)}, p_k^{(s,v)}\right)\right\}_{v=1}^{M_k^{(s)}}$ with $p_k^{(s,v)}=\sum_{i=1}^{J_k^{(s,v)}}\omega_{k,i}^{(s,v)}\cdot\sum_{m=1}^{N}u_{k,i,m}^{(s,v)}\mathcal{N}(\boldsymbol{x};\boldsymbol{m}_{k,i,m}^{(s,v)}, \boldsymbol{P}_{k,i,m}^{(s,v)})$, $s=0, 1, \cdots, S$, as described in Eqs. (1) and (2).

Every BC $\left(r_k^{(s,v)}, p_k^{(s,v)}\right)$ characterizes a potential target that features the following state estimate and error covariance:

$$\hat{\boldsymbol{x}}_{\mathrm{BC},k}^{(s,v)}=\sum_{i=1}^{J_k^{(s,v)}}\omega_{k,i}^{(s,v)}\hat{\boldsymbol{x}}_{\mathrm{JMGM},k,i}^{(s,v)}, \tag{22}$$

$$\begin{aligned}\boldsymbol{P}_{\mathrm{BC},k}^{(s,v)}=&\sum_{i=1}^{J_k^{(s,v)}}\omega_{k,i}^{(s,v)}[\boldsymbol{P}_{\mathrm{JMGM},k,i}^{(s,v)}\\ &+(\hat{\boldsymbol{x}}_{\mathrm{JMGM},k,i}^{(s,v)}-\hat{\boldsymbol{x}}_k^{(s,v)})(\hat{\boldsymbol{x}}_{\mathrm{JMGM},k,i}^{(s,v)}-\hat{\boldsymbol{x}}_k^{(s,v)})^{\mathrm{T}}],\end{aligned} \tag{23}$$

where $\hat{\boldsymbol{x}}_{\mathrm{JMGM},k,i}^{(s,v)}$ and $\boldsymbol{P}_{\mathrm{JMGM},k,i}^{(s,v)}$ are the estimate and error covariance of the i^{th} JMGM component, respectively, i.e.,

$$\hat{\boldsymbol{x}}_{\mathrm{JMGM},k,i}^{(s,v)}=\sum_{m=1}^{N}u_{k,i,m}^{(s,v)}\boldsymbol{m}_{k,i,m}^{(s,v)}, \tag{24}$$

$$\begin{aligned}\boldsymbol{P}_{\mathrm{JMGM},k,i}^{(s,v)}=&\sum_{m=1}^{N}u_{k,i}^{(s,v)}[\,\boldsymbol{P}_{k,i,m}^{(s,v)}\\&+(\boldsymbol{m}_{k,i,m}^{(s,v)}-\hat{\boldsymbol{x}}_{k,i}^{(s,v)})(\boldsymbol{m}_{k,i,m}^{(s,v)}-\hat{\boldsymbol{x}}_{k,i}^{(s,v)})^{\mathrm{T}}\,].\end{aligned} \tag{25}$$

Each filter estimates the target number via

$$\hat{N}_k^{(s)}=\mathrm{round}\left(\sum_{v=1}^{M_k^{(s)}}r_k^{(s,v)}\right), \tag{26}$$

with the rounding-off operation round$(\cdot)$. Then, each filter extracts $\hat{N}_k^{(s)}$ BCs with the largest existence probabilities and regards them as target-like BCs (T-BCs). These T-BCs are sent to the fusion node, waiting for association and merging. The reason for handling only T-BCs but not all BCs has been fully discussed in Li TC et al. (2019a).

3. Association and merging

When collecting the T-BCs above, the fusion node labels them with their filter indices and assigns an average factor $\beta(s)$ to each filter $\left(\sum_{s=0}^{S}\beta(s)=1\right)$. These average factors quantify the relative reliabilities of the master and local filters.

All collected T-BCs are uniformly recorded as

$$\{(r_{\mathrm{T},k}^{(v)},p_{\mathrm{T},k}^{(v)},l_{\mathrm{T},k}^{(v)})\}_{v=1}^{\sum_{s=0}^{S}\hat{N}_k^{(s)}}, \tag{27}$$

where $r_{\mathrm{T},k}^{(v)}$ and $p_{\mathrm{T},k}^{(v)}$ are the existence probability and state PDF of the v^{th} T-BC, respectively, and $l_{\mathrm{T},k}^{(v)}\in\{0, 1, \cdots, S\}$ is its filter index label.

Association of T-BCs: For two T-BCs with superscripts v and u, if their squared Mahalanobis distance satisfies

$$(\tilde{\boldsymbol{x}}_k^{(vu)})^{\mathrm{T}}(\boldsymbol{P}_k^{(v)}+\boldsymbol{P}_k^{(u)})^{-1}\tilde{\boldsymbol{x}}_k^{(vu)}+1[\,l_{\mathrm{T},k}^{(v)}=l_{\mathrm{T},k}^{(u)}]\cdot\lambda_{\mathrm{m}}<\lambda_{\mathrm{m}}, \tag{28}$$

then they will be regarded as originating from the same potential target state, where $\hat{\boldsymbol{x}}_k^{(v)}$ and $\boldsymbol{P}_k^{(v)}$ are the estimate and error covariance of the v^{th} T-BC respectively, as computed via Eqs. (22)–(25). The estimate residual $\tilde{\boldsymbol{x}}_k^{(vu)}=\hat{\boldsymbol{x}}_k^{(v)}-\hat{\boldsymbol{x}}_k^{(u)}$; the indicator $1[\cdot]=1$ when the condition $[\cdot]$ is met, and $1[\cdot]=0$ otherwise.

The reason for adopting the distance computation above is to prevent associating and merging T-BCs of the same filter: Adding $1[\,l_{\mathrm{T},k}^{(v)}=l_{\mathrm{T},k}^{(u)}]\cdot\lambda_{\mathrm{m}}$ forces the distances of T-BCs of the same filter to be larger than λ_{m}, making it impossible to associate and merge them. Based on the distance computation above, the association task of T-BCs can be achieved using the k-means clustering method (Li TC et al., 2018).

Suppose that all T-BCs in expression (27) are associated into G_k groups, meaning that the fusion node assumes that, at most, G_k targets exist. The association operation above decomposes multi-target fusion into multiple groups of single-target fusion.

Merging of T-BCs: Let $\mathcal{S}_k^{(v)}\subseteq\left\{1, 2, \cdots, \sum_{s=0}^{S}\hat{N}_k^{(s)}\right\}$ denote the superscripts of the v^{th} group of associated T-BCs. Then their filter index labels are

$$\mathcal{L}_k^{(v)}=\bigcup_{u\in\mathcal{S}_k^{(v)}}l_{\mathrm{T},k}^{(u)}. \tag{29}$$

Each group of associated T-BCs is merged into one new BC with the following existence probability and state PDF:

$$r_k^{(\mathrm{F},v)}=\sum_{u\in\mathcal{S}_k^{(v)}}\beta(l_{\mathrm{T},k}^{(u)})r_{\mathrm{T},k}^{(u)}, \tag{30}$$

$$p_k^{(\mathrm{F},v)}=\frac{\sum_{u\in\mathcal{S}_k^{(v)}}\beta(l_{\mathrm{T},k}^{(u)})r_{\mathrm{T},k}^{(u)}p_{\mathrm{T},k}^{(u)}}{\sum_{u\in\mathcal{S}_k^{(v)}}\beta(l_{\mathrm{T},k}^{(u)})r_{\mathrm{T},k}^{(u)}}, \tag{31}$$

where $l_{\mathrm{T},k}^{(u)}\in\{0, 1, \cdots, S\}$ and $\beta(l_{\mathrm{T},k}^{(u)})$ is the average factor assigned to filter $l_{\mathrm{T},k}^{(u)}$.

Merging of T-JMGM components: The highest weighted JMGM component of a T-BC is called a target-like JMGM (T-JMGM) component. The v^{th} group of associated T-BCs incorporates $|\mathcal{L}_k^{(v)}|$ T-JMGM components with the set cardinality $|\cdot|$, and they are recorded as

$$\left\{\omega_{\mathrm{T},k,i}^{(v)},\left(u_{\mathrm{T},k,i,m}^{(v)},\boldsymbol{m}_{\mathrm{T},k,i,m}^{(v)},\boldsymbol{P}_{\mathrm{T},k,i,m}^{(v)}\right)_{m=1}^{N}\right\}_{i=1}^{|\mathcal{L}_k^{(v)}|}, \tag{32}$$

where the i^{th} T-JMGM component features a weight $\omega_{\mathrm{T},k,i}^{(v)}$ and N model-conditioned probabilities $u_{k,i,m}^{(v)}$, means $\boldsymbol{m}_{\mathrm{T},k,i,m}^{(v)}$, and covariances $\boldsymbol{P}_{\mathrm{T},k,i,m}^{(v)}$.

These T-JMGM components are state estimates of the same target and, thus, should be merged into one. The weight of the merged JMGM component is

$$\omega=\sum_{i=1}^{|\mathcal{L}_k^{(v)}|}\beta\left(\mathcal{L}_k^{(v)}(i)\right)\omega_{\mathrm{T},k,i}^{(v)}, \tag{33}$$

where $\mathcal{L}_k^{(v)}(i)\in\{0,1,\cdots,S\}$ is the i^{th} element of $\mathcal{L}_k^{(v)}$.

The fusion node is capable of identifying the origin of associated T-BCs using the filter index labels $\mathcal{L}_k^{(v)}$, and accordingly adopts a particular merging method for the model-conditioned probabilities, means, and covariances in expression (32).

(1) Survival target without missed detections: $|\mathcal{L}_k^{(v)}|=S+1$, i.e., $\mathcal{L}_k^{(v)}=\{0,1,\cdots,S\}$, which means that the master and local filters capture a target that already exists. According to the optimal fusion of a single maneuvering target in the absence of missed detections, as given in Eqs. (12)–(14) of Section 3.1, the model-conditioned quantities in expression (32) are merged in the following CC form:

$$u_m=\frac{\prod_{i=1}^{|\mathcal{L}_k^{(v)}|}u_{\mathrm{T},k,i,m}^{(v)}/\left(u_{\mathrm{T},k,r,m}^{(v)}\right)^{|\mathcal{L}_k^{(v)}|-1}}{\sum_{m=1}^{N}\prod_{i=1}^{|\mathcal{L}_k^{(v)}|}u_{\mathrm{T},k,i,m}^{(v)}/\left(u_{\mathrm{T},k,r,m}^{(v)}\right)^{|\mathcal{L}_k^{(v)}|-1}} \quad \text{s.t.}\ \ \mathcal{L}_k^{(v)}(r)=0, \tag{34}$$

$$\boldsymbol{m}_m=\boldsymbol{P}_m\cdot\sum_{i=1}^{|\mathcal{L}_k^{(v)}|}\left(\boldsymbol{P}_{\mathrm{T},k,i,m}^{(v)}\right)^{-1}\boldsymbol{m}_{\mathrm{T},k,i,m}^{(v)}, \tag{35}$$

$$\boldsymbol{P}_m^{-1}=\sum_{i=1}^{|\mathcal{L}_k^{(v)}|}\left(\boldsymbol{P}_{\mathrm{T},k,i,m}^{(v)}\right)^{-1}. \tag{36}$$

(2) Survival target with missed detections: $1<|\mathcal{L}_k^{(v)}|<S+1$, and 0 exists in $\mathcal{L}_k^{(v)}$, which means that some but not all local filters miss a survival target, while others and the master filter capture it. According to the optimal single-target fusion in the presence of missed detections, as given in Eqs. (15) and (16) of Section 3.2, the model probabilities in expression (32) are merged as per Eq. (34), while the means and covariances are merged via

$$\boldsymbol{m}_m=\boldsymbol{P}_m\left[\sum_{i=1}^{|\mathcal{L}_k^{(v)}|}\left(\boldsymbol{P}_{\mathrm{T},k,i,m}^{(v)}\right)^{-1}\boldsymbol{m}_{\mathrm{T},k,i,m}^{(v)}+\sum_{r\in\{0,1,\cdots,S\}\setminus\mathcal{L}_k^{(v)}}\left(\boldsymbol{\mathcal{C}}_{k|k-1,r,m}^{(v)}\right)^{-1}\boldsymbol{\xi}_{k|k-1,r,m}^{(v)}\right], \tag{37}$$

$$\boldsymbol{P}_m^{-1}=\sum_{i=1}^{|\mathcal{L}_k^{(v)}|}\left(\boldsymbol{P}_{\mathrm{T},k,i,m}^{(v)}\right)^{-1}+\sum_{r\in\{0,.1,\cdots,S\}\setminus\mathcal{L}_k^{(v)}}\left(\boldsymbol{\mathcal{C}}_{k|k-1,r,m}^{(v)}\right)^{-1}, \tag{38}$$

where filter r misses the survival target mentioned above and fails to provide a T-BC, $r\in\{0,1,\cdots,S\}\setminus\mathcal{L}_k^{(v)}$, $\{\cdot\}\setminus\{\cdot\}$ is the set difference, and $\boldsymbol{\xi}_{k|k-1,r,m}^{(v)}$ and $\boldsymbol{\mathcal{C}}_{k|k-1,r,m}^{(v)}$ are the predicted mean and covariance of filter r respectively, which can be supplemented via

$$\begin{cases}\boldsymbol{\xi}_{k|k-1,r,m}^{(v)}=\boldsymbol{m}_{\mathrm{T},k,i,m}^{(v)},\\ \boldsymbol{\mathcal{C}}_{k|k-1,r,m}^{(v)}=\beta(0)/\beta(r)\cdot\boldsymbol{P}_{\mathrm{T},k,i,m}^{(v)},\end{cases}\quad\text{s.t.}\ \mathcal{L}_k^{(v)}(i)=0. \tag{39}$$

(3) Newborn target: $1<|\mathcal{L}_k^{(v)}|<S+1$, but 0 does not exist in $\mathcal{L}_k^{(v)}$, which means that some or all local filters capture a newborn target, while the master filter does not know it yet due to the lack of observation data. To reduce the effect of unknown correlations among newborn target estimates, the model probabilities, means, and covariances in expression (32) are merged using the CI fusion, i.e.,

$$u_m=\frac{\sum_{i=1}^{|\mathcal{L}_k^{(v)}|}\omega_{\mathrm{T},k,i,m}^{(v)}u_{\mathrm{T},k,i,m}^{(v)}}{\sum_{m=1}^{N}\sum_{i=1}^{|\mathcal{L}_k^{(v)}|}\omega_{\mathrm{T},k,i,m}^{(v)}u_{\mathrm{T},k,i,m}^{(v)}}, \tag{40}$$

$$\boldsymbol{m}_m=\boldsymbol{P}_m\cdot\left[\sum_{i=1}^{|\mathcal{L}_k^{(v)}|}\omega_{\mathrm{T},k,i}^{(v)}\left(\boldsymbol{P}_{\mathrm{T},k,i,m}^{(v)}\right)^{-1}\boldsymbol{m}_{\mathrm{T},k,i,m}^{(v)}\right]\Big/\omega, \tag{41}$$

$$\boldsymbol{P}_m^{-1}=\sum_{i=1}^{|\mathcal{L}_k^{(v)}|}\omega_{\mathrm{T},k,i,m}^{(v)}\left(\boldsymbol{P}_{\mathrm{T},k,i,m}^{(v)}\right)^{-1}\Big/\omega. \tag{42}$$

(4) Vanishing target: $\mathcal{L}_k^{(v)}=\{0\}$, which means that all local filters find a target that has vanished, while the master filter does not know it yet due to the lack of observation data and still maintains its T-BC. In this situation, this T-BC and its JMGM components are discarded.

Our algorithm is capable of judging the origin of associated T-BCs in expression (27) based on the filter index labels $\mathcal{L}_k^{(v)}$: survival targets with or without missed detections, newborn targets, or vanishing targets. Each situation employs a particular method to merge T-JMGM components. This origin-conditioned merging method is the core of our algorithm, which is provided in the supplementary materials.

The merged BCs with existence probabilities smaller than $\lambda_{\mathrm{d}}^{\mathrm{BC}}$ and JMGM components with weights smaller than $\lambda_{\mathrm{d}}^{\mathrm{JMGM}}$ are discarded. To the end, the fused multi-target density at time k is recorded as $\pi_k^{(\mathrm{F})}=\{(r_k^{(\mathrm{F},v)},p_k^{(\mathrm{F},v)})\}_{v=1}^{M_k^{(\mathrm{F})}}$ $(M_k^{(\mathrm{F})}\le G_k)$ with existence

probabilities $r_k^{(\mathrm{F},v)}$ and state PDFs in the following JMGM form:

$$p_k^{(\mathrm{F},v)}=\sum_{i=1}^{J_k^{(\mathrm{F},v)}}\omega_{k,i}^{(\mathrm{F},v)}\sum_{m=1}^{N}u_{k,i,m}^{(\mathrm{F},v)}\mathcal{N}(\boldsymbol{x};\boldsymbol{m}_{k,i,m}^{(\mathrm{F},v)},\boldsymbol{P}_{k,i,m}^{(\mathrm{F},v)}). \quad (43)$$

4.3 Cardinality consensus

In the proposed fusion algorithm, only T-BCs are merged, not all BCs. Consequently, the target number (also known as cardinality), which is reflected in the sum of all BCs' existence probabilities, tends to be underestimated.

To remedy this cardinality bias, we adopt three measures to guarantee cardinality consensus.

Measure-1: When the master and local filters send their T-BCs to the fusion node, each filter apportions its cardinality over T-BCs via

$$r_{\mathrm{T},k}^{(v)}=\frac{\sum_{s=0}^{S}\beta(s)\sum_{v=1}^{M_k^{(s)}}r_k^{(s,v)}}{\sum_{v=1}^{\hat{N}_k^{(s)}}r_{\mathrm{T},k}^{(v)}}r_{\mathrm{T},k}^{(v)},\ v=1,2,\cdots,\hat{N}_k^{(s)}, \quad (44)$$

where $\sum_{v=1}^{M_k^{(s)}}r_k^{(s,v)}$ is the estimated target cardinality of filter s with the existence probabilities of $M_k^{(s)}$ BCs $r_k^{(s,v)}$, and $r_{\mathrm{T},k}^{(v)}$ is the existence probability of the v^{th} T-BC.

Measure-2: When the fused density is assigned to the master and local filters, as shown in Eq. (19), each filter modifies its cardinality via

$$r_{k-1}^{(s,v)}=\frac{\sum_{v=1}^{M_{k-1}^{(\mathrm{F})}}r_{k-1}^{(\mathrm{F},v)}}{\sum_{v=1}^{M_{k-1}^{(s)}}r_{k-1}^{(s,v)}}r_{k-1}^{(s,v)},\quad v=1,2,\cdots,M_{k-1}^{(s)}, \quad (45)$$

where $\sum_{v=1}^{M_{k-1}^{(\mathrm{F})}}r_{k-1}^{(\mathrm{F},v)}$ is the estimated target cardinality of fused density with its existence probability $r_{k-1}^{(\mathrm{F},v)}$.

Measure-3: The two measures above may lead to some existence probabilities r being larger than 1. This not only violates the definition of probabilities but also causes severe errors as the updating operations of weights and existence probabilities involve coefficients $r/(1-r)$ and $r(1-r)$. Hence, the existence probabilities in Eqs. (44) and (45) must be limited to less than 1 via

$$r=\frac{r}{\max(\max r,1)+\partial}, \quad (46)$$

where an infinitesimal value ∂ such as "eps" in MATLAB ensures $r<1$ instead of $r\le 1$, and $\max(\max r,1)$ would cause existence probabilities larger than 1 to decrease but does not affect those smaller than 1.

4.4 Average factors and algorithm summary

Average factors: Average factors quantify the relative reliabilities of the master and local filters. For the local filters ($s=1,2,\cdots,S$), their average factors rely on the performance of sensor nodes.

For the master filter ($s=0$), a small average factor is preferred. The reasons are given as follows:

1. The fusion node cannot sense targets, and the master filter predicts only the fused multi-target density. Therefore, the average factor of the master filter should be smaller than that of local filters, i.e., $\beta(0)<\beta(s)$, $\forall s\in\{1,2,\cdots,S\}$.

2. A persistent underestimation of the target number may arise from a large average factor of the master filter. Recalling Eq. (30), the existence probabilities of associated T-BCs are merged via weighted sum. For newborn targets, the absence of the master filter's T-BC causes the merged existence probability to be smaller than 1. The larger $\beta(0)$ is, the smaller the merged existence probability is. Even the newborn target BC may be regarded as a false alarm. Even worse, the master filter cannot remedy this incorrect fusion result due to the lack of observation data, leading to the absence of the master filter's T-BC again. This cross-contamination between the fusion node and the master filter tends to cause a persistent underestimation of the target number.

Algorithm summary: This paper achieves the optimal decentralized fusion of JMGM-MB filters in a hierarchical network. We provide the procedure of the proposed federated fusion of JMGM-MB filters in Algorithm 1.

5 Numerical results

This section compares the proposed federated fusion with the MM-GM-MB filter, the JMGM-MB filter, the centralized PM fusion of JMGM-MB filters, and the distributed AA fusion of JMGM-MB filters.

5.1 Setup

We design three maneuvering targets, with initial states $\boldsymbol{x}_1^{(1)}$=[600 m, 900 m, 10 m/s, −10 m/s]$^{\mathrm{T}}$, $\boldsymbol{x}_1^{(2)}$=[500 m, 500 m, 10 m/s, 3 m/s]$^{\mathrm{T}}$, and $\boldsymbol{x}_1^{(3)}$=[400 m, 600 m, 20 m/s, 4 m/s]$^{\mathrm{T}}$. Target-1 exists during [2, 100] s, governed by the constant velocity (CV) model for 59 s + the anti-clockwise coordinated turning (ACT) model for 21 s + the CV model for 19 s. Target-2 exists during [13, 90] s, governed by the CV model for 39 s + the ACT model for 39 s. Target-3 keeps the CV model during [25, 60] s. All models are polluted by process noises with the same covariance $\boldsymbol{Q}$=diag(1, 1, 0.01, 0.01). The sampling period T=1 s.

In all filtering/fusion algorithms, the pruning thresholds of BCs and JMGM components are, respectively, $\lambda_{\mathrm{d}}^{\mathrm{BC}}$=0.001 and $\lambda_{\mathrm{d}}^{\mathrm{JMGM}}$=0.001, and the full merging threshold is λ_{m}=4. N=2 possible models include the CV model (m=1) and the ACT model (m=2), and the Markovian transition probability u_{mn}=0.02 ($m\neq n$). At each iteration, every JMGM-MB filter introduces three newborn target BCs with the same existence probability of 0.033. The state PDFs of these BCs incorporate 300 JMGM components, the means of which are randomly distributed within $\boldsymbol{x}_1^{(v)}$+[−10 −10 −1 −1]$^{\mathrm{T}}$ (lower bound) and $\boldsymbol{x}_1^{(v)}$+[10 10 1 1]$^{\mathrm{T}}$ (upper bound), v=1, 2, 3; they share the same weight 0.01, model probability [0.5, 0.5]$^{\mathrm{T}}$, and covariance diag(10, 10, 4, 4).

The optimal sub-pattern assignment (OSPA) error (Schuhmacher et al., 2008) is used to quantify the tracking performance of a time-varying number of maneuvering targets, with cutoff parameter c=10 and order parameter p=2.

5.2 Single-target linear fusion

First, we plan to reveal an issue of the conventional sequential fusion: since the estimates of different models are more similar to the truth, as more sensor measurements are fused, the difference in likelihood becomes smaller. The measurements fused later barely modify the model probabilities further, as if their likelihoods were fading out. This may cause only a very small bias as model probabilities are already concentrated on the true model, but this abovementioned issue is still counterintuitive. In the Bayesian fusion, likelihoods are always computed based on the

Algorithm 1 Federated fusion of JMGM-MB filters

1. Assign fused BCs, process noise covariance, and distance threshold to each filter as per Eqs. (19)–(21), where existence probabilities are modified as per $r_{k-1}^{(s,v)}=r_{k-1}^{(s,v)}\sum_{v=1}^{M_{k-1}^{(\mathrm{F})}} r_{k-1}^{(\mathrm{F},v)} \Big/ \sum_{v=1}^{M_{k-1}^{(s)}} r_{k-1}^{(s,v)}$ and $r=r/(\max(\max r, 1)+\partial)$.
2. S local filters perform full JMGM-MB filtering, while the master filter performs only prediction. Their posterior MBs are recorded as $\pi_k^{(s)}=\{(r_k^{(s,v)}, p_k^{(s,v)})\}_{v=1}^{M_k^{(s)}}$ with $p_k^{(s,v)}=\sum_{i=1}^{J_k^{(s,v)}}\omega_{k,i}^{(s,v)}\sum_{m=1}^{N}u_{k,i,m}^{(s,v)}\mathcal{N}(\boldsymbol{x};\boldsymbol{m}_{k,i,m}^{(s,v)},\boldsymbol{P}_{k,i,m}^{(s,v)})$.
3. Each filter extracts $\hat{N}_k^{(s)}=\mathrm{round}\left(\sum_{v=1}^{M_k^{(s)}} r_k^{(s,v)}\right)$ T-BCs, apportions existence probabilities as per $r_{\mathrm{T},k}^{(v)}=r_{\mathrm{T},k}^{(v)}\sum_{s=0}^{S}\beta(s)\sum_{v=1}^{M_k^{(s)}} r_k^{(s,v)} \Big/ \sum_{v=1}^{\hat{N}_k^{(s)}} r_{\mathrm{T},k}^{(v)}$, $r=r/(\max(\max r, 1)+\partial)$, and sends them to the fusion node.
4. All received T-BCs $\{(r_{\mathrm{T},k}^{(v)}, p_{\mathrm{T},k}^{(v)}, l_{\mathrm{T},k}^{(v)})\}_{v=1}^{\sum_{s=0}^{S}\hat{N}_k^{(s)}}$ are associated into G_k groups as per $(\tilde{\boldsymbol{x}}_k^{(vu)})^{\mathrm{T}}(\boldsymbol{P}_k^{(v)}+\boldsymbol{P}_k^{(u)})^{-1}\tilde{\boldsymbol{x}}_k^{(vu)}+1[l_{\mathrm{T},k}^{(v)}=l_{\mathrm{T},k}^{(u)}]\cdot\lambda_{\mathrm{m}}<\lambda_{\mathrm{m}}$.
5. Each group of associated BCs is merged as per $p_k^{(\mathrm{F},v)}=\sum_u\beta(l_{\mathrm{T},k}^{(u)})r_{\mathrm{T},k}^{(u)}p_{\mathrm{T},k}^{(u)} \Big/ \sum_u\beta(l_{\mathrm{T},k}^{(u)})r_{\mathrm{T},k}^{(u)}$ and $r_k^{(\mathrm{F},v)}=\sum_u\beta(l_{\mathrm{T},k}^{(u)})r_{\mathrm{T},k}^{(u)}$, $u\in\mathcal{S}_k^{(v)}$.
6. Extract T-JMGM components $\{\omega_{\mathrm{T},k,i}^{(v)}, (u_{\mathrm{T},k,i,m}^{(v)}, \boldsymbol{m}_{\mathrm{T},k,i,m}^{(v)}, \boldsymbol{P}_{\mathrm{T},k,i,m}^{(v)})_{m=1}^{N}\}_{i=1}^{|\mathcal{L}_k^{(v)}|}$, and merge their weights as per $\omega=\sum_{i=1}^{|\mathcal{L}_k^{(v)}|}\beta(\mathcal{L}_k^{(v)}(i))\omega_{\mathrm{T},k,i}^{(v)}$.

   Different association situations employ particular methods to merge their model probabilities, means, and covariances.

   Situation 1 Survival target without missed detections: use CC fusion in Eqs. (34)–(36).

   Situation 2 Survival target with missed detections: supplement missed detections using Eq. (39) and then operate CC fusion in Eqs. (34), (37), and (38).

   Situation 3 Newborn target: use CI fusion in Eqs. (40)–(42).

   Situation 4 Vanishing target: discard this T-BC.
7. Extract $\hat{N}_k=\mathrm{round}\left(\sum_{v=1}^{M_k^{(\mathrm{F})}} r_k^{(\mathrm{F},v)}\right)$ BCs with the largest existence probabilities, and their state estimates are computed as per Eqs. (22)–(25).

prior model-conditioned densities. The measurements of all sensors are treated equally as evidence of the true model, regardless of the fusion order.

In a scenario involving the designed target-1 and S=9 sensor nodes, the average position error of the Bayesian fusion is 7.01% smaller than that of the sequential fusion. The conventional sequential fusion of IMM filters and the single-target tracking result are provided in the supplementary materials.

5.3 Multi-target linear fusion

Next, we test the proposed federated fusion in the intact multi-target scenarios in Section 5.1. We simulate S=3 linear sensor nodes with the same observation model. They share the same detection range of (x-axis) [200, 1800] m×(y-axis) [200, 1000] m. Their observation is polluted by clutters with a density of $\kappa^{(s)}=2\times10^{-6}$ m^{-2} (the statistical average of clutter numbers is 2.56 per second) and missed detections with a probability of $1-p_{\mathrm{D}}^{(s)}=2\%$, $s=1,2,3$. The sensor weights in the AA fusion are $\alpha(s)=1/3$, $s=1,2,3$. The average factors in the federated fusion are $\beta(0)=1/31$ and $\beta(1)=\beta(2)=\beta(3)=10/31$.

Table 1 provides the missed detection logs of the three sensor nodes, which record the instants at which missed detections occur. These logs are only used to analyze simulations but are unavailable to all algorithms. The tracking results are shown in Fig. 2. Fig. 3 plots the model probability error curves of different algorithms. Figs. 4 and 5 plot the estimates of T-BCs associated at 13 and 40 s, respectively. The target number estimation and OSPA error curves of different algorithms are given in Figs. 6 and 7, respectively. After 200 Monte Carlo runs, Table 2 records the average mean, standard deviation (std), and maximum (max) of each algorithm's OSPA error.

Fig. 2 illustrates that the designed scenario involves not only significant target maneuvers but also multiple intersections of target trajectories. In this situation, all algorithms still exhibit stable tracking results. For the fusion tracking of multiple maneuvering targets, accurate model probability estimation and estimate association are indispensable conditions. As seen in Fig. 3, the proposed federated fusion yields the lowest model probability error, even lower than that of the PM fusion. As seen in Fig. 4, two groups of

Table 1 Missed detection log of each sensor node

Sensor node index	Instants at which missed detections occur
1	11, 46, 99 s
2	18, 22 s
3	15, 33, 35, 51, 90 s

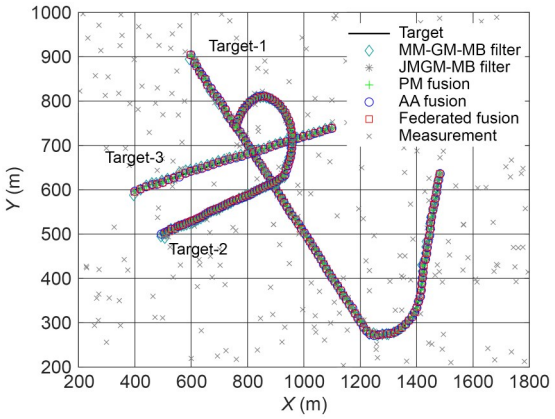

Fig. 2 Tracking results of different algorithms

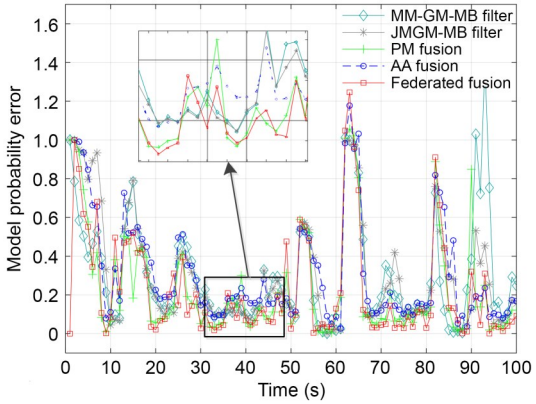

Fig. 3 Multi-target model probability error curves of different algorithms

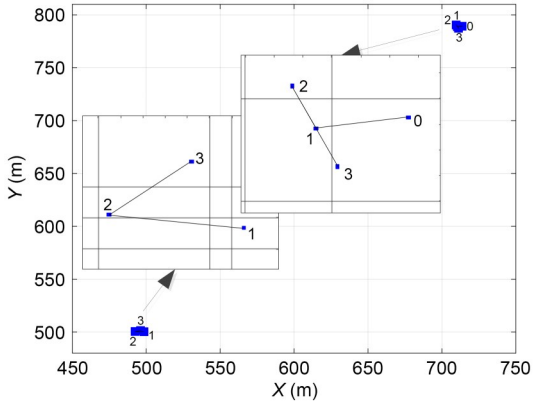

Fig. 4 Estimates of T-BCs associated at 13 s

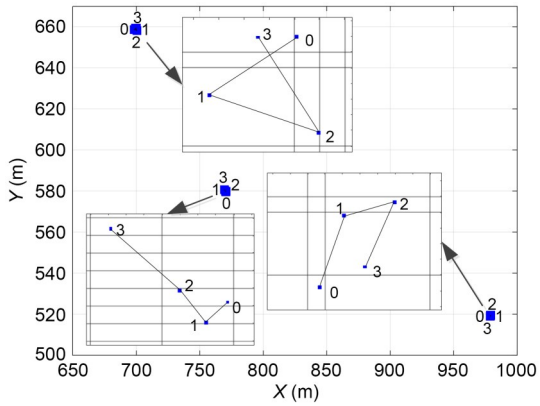

Fig. 5 Estimates of T-BCs associated at 40 s

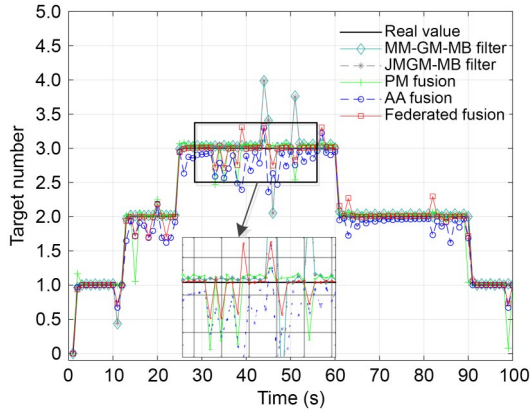

Fig. 6 Target number estimation of different algorithms

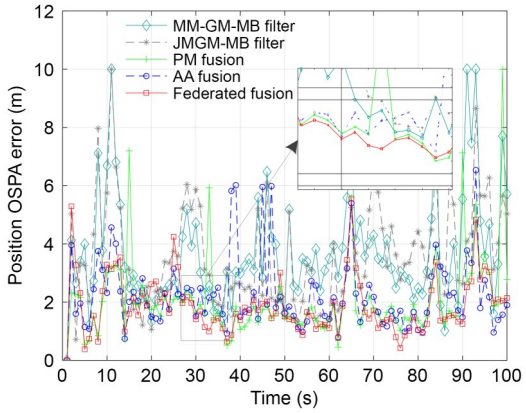

Fig. 7 OSPA error curves of different algorithms

estimates of associated T-BCs at 13 s feature filter index labels "1, 2" and "1, 2, 3," which conform to the new birth of target-2 and the survival of target-3, respectively. In Fig. 5, all three groups of filter index labels are "1, 2, 3," which conform to the existence of all three targets at 40 s. In other words, our algorithm is capable of accurately associating T-BCs of the same target and identifying their origin using the filter index labels. The latter is impossible with the existing density fusion. The accuracy of estimate association will not be affected by missed detections since the master filter can supplement missed detections. Satisfying the two abovementioned conditions indicates optimal tracking accuracy. In Fig. 6, AA fusion tends to underestimate the target number, largely because only T-BCs are handled, ignoring the existence probabilities of other BCs. In contrast, our algorithm adopts the measures in Section 4.3 to guarantee cardinality consensus. Other algorithms exhibit acceptable target number estimation. As seen in Fig. 7, the JMGM-MB filter outperforms the conventional MM-GM-MB filter, and all fusion algorithms outperform the single-sensor JMGM-MB filter. According to the logs in Table 1, all performance deterioration of the PM fusion occurs with missed detections, which means it is relatively sensitive to missed detections. AA fusion fails to eliminate correlations. In contrast, the proposed fusion algorithm exhibits the lowest OSPA error curve by virtue of its ability to supplement missed detections and eliminate correlations. The statistics in Table 2 further support the conclusions above: Compared to the federated fusion, the OSPA error means of the PM and AA fusion are higher by 7.03% and 12.75%, respectively.

Table 2 Statistics of different algorithms

Algorithm	OSPA error (m)		
	Mean	Std	Max
MM-GM-MB	4.0270	1.8913	9.9564
JMGM-MB	3.4459	1.7557	9.0112
PM fusion	2.1469	1.1764	7.3776
AA fusion	2.2615	1.2589	8.0627
Federated fusion	2.0058	0.9422	6.0762

To verify the effectiveness of the measures for cardinality consensus and the analyses of the average factor of the master filter $\beta(0)$, as given in Sections 4.3 and 4.4, we compare three editions of the federated fusion: (a) the setup is the same as in Section 5.1 ($\beta(0)$ is small) and the measures in Section 4.3 are adopted; (b) the setup is the same as in Section 5.1 but the measures in Section 4.3 are deleted; (c) a large

$\beta(0)=1/2$ is used ($\beta(s)=1/6$, $s=1, 2, 3$) but the measures above are adopted. Fig. 8 provides their target number estimation and OSPA error curves.

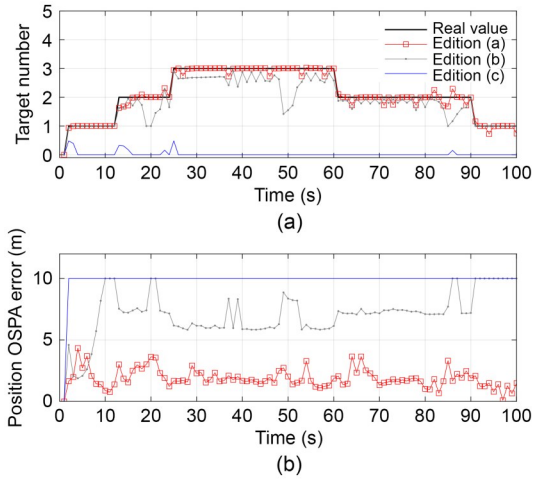

Fig. 8 Estimated target number (a) and OSPA error (b) curves of three editions of the federated fusion

As we can see, editions (b) and (c) suffer from significant underestimations of the target number. The measures in Section 4.3 apportion the existence probabilities of all BCs over T-BCs, thereby remedying the target cardinality. The master filter, with a large average factor, tends to cause missed detections and maintain incorrect target number estimation. As a result, the absence of the measures in Section 4.3 or a large average factor of the master filter can lead to a persistent underestimation of the target number.

Observing the optimal single-target fusion in Section 3, we find that adjusting average factors $\beta(s)$ will not jeopardize the optimality as long as they are reasonable and satisfy $\sum_{s=0}^{S}\beta(s)=1$. This is also why the master filter is required to supplement missed detections (to supplement missed average factor to ensure $\sum_{s=0}^{S}\beta(s)=1$). To verify the reconfigurability of average factors, we adopt a set of time-varying average factors: $\beta(0)=1/31$ and $\beta(1)=\beta(2)=\beta(3)=10/31$ during [1, 29] s; $\beta(0)=1/41$, $\beta(1)=20/41$, and $\beta(2)=\beta(3)=10/41$ during [30, 59] s; $\beta(0)=1/51$, $\beta(1)=\beta(2)=20/51$, and $\beta(3)=10/51$ during [60, 100] s. Other parameters are the same as in Section 5.1. Fig. 9 provides the OSPA error curves of the federated fusion and three local filters.

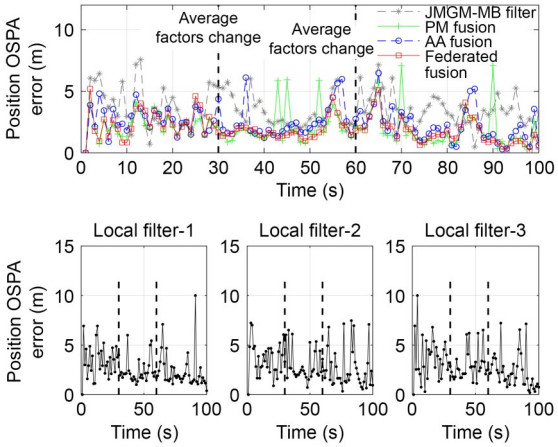

Fig. 9 OSPA error curves when average factors are time-varying

Obviously, since the observation performance of sensor nodes does not change, the OSPA error curves of the federated fusion and three local filters do not fluctuate with average factors. This parameter reconfigurability can engender better adaptability. For instance, the average factor of a sensor node can increase as this sensor approaches targets.

5.4 Multi-target heterogeneous fusion

Next, we test the federated fusion in a scenario involving an active sensor and a passive sensor ($S=2$).

The active sensor ($s=1$) is fixed at the origin of the global coordinate system and captures targets of interest via

$$\boldsymbol{z}^{(1)}=h^{(1)}(\boldsymbol{x})+\boldsymbol{v}^{(1)}=\begin{bmatrix}\sqrt{x^2+y^2}\\ \arctan(x/y)\end{bmatrix}+\boldsymbol{v}^{(1)}, \quad (47)$$

where (x, y) is the position of $\boldsymbol{x}$, $h^{(1)}$ is the active sensor's observation function, and the mean and covariance of Gaussian noise $\boldsymbol{v}^{(1)}$ are $\boldsymbol{0}$ and $\boldsymbol{R}^{(1)}=\mathrm{diag}(25, 1)$, respectively.

A moving sensor is necessary to satisfy the observability in bearings-only tracking, so the passive sensor ($s=2$) keeps moving towards the mean of bearings-only measurements. Let $(x^{\mathrm{O}}, y^{\mathrm{O}})$ and θ^{O} denote the position and observation angle of this moving passive sensor in the global coordinate system respectively, where the observation angle is positive clockwise with respect to the global Y axis. From the sensor's perspective, the target features the following state:

$$\boldsymbol{x}'=\boldsymbol{C}(\boldsymbol{x}-\boldsymbol{t}),\quad \boldsymbol{C}=\mathrm{blkdiag}(\boldsymbol{c},\boldsymbol{c}),\tag{48}$$

where blkdiag( ) represents the block diagonal matrix, $\boldsymbol{t}=[\,x^{\mathrm{O}},y^{\mathrm{O}},0,0\,]^{\mathrm{T}}$ is the state translation vector, and $\boldsymbol{c}=\begin{bmatrix}\cos\theta^{\mathrm{O}} & -\sin\theta^{\mathrm{O}}\\ \sin\theta^{\mathrm{O}} & \cos\theta^{\mathrm{O}}\end{bmatrix}$ is the coordinate rotation matrix. This passive sensor provides the bearings-only measurements via the following observation model:

$$z^{(2)}=h^{(2)}(\boldsymbol{x}')+v^{(2)}=\arctan(x'/y')+v^{(2)},\tag{49}$$

where (x',y') is the position of $\boldsymbol{x}'$, $h^{(2)}$ is the passive sensor's observation function, and the mean and covariance of Gaussian noise $v^{(2)}$ are 0 and $R^{(2)}=1$, respectively.

The detection ranges of the active and passive sensors are (range) [400, 1800] m×(bearing) [0°, 90°] and (bearings-only) [−60°, 60°], respectively. All bearing angles are positive clockwise with respect to the sensors' Y axes. The clutter densities of the active and passive sensors are $k^{(1)}=8\times10^{-6}$ m^{-1}(°)$^{-1}$ and $k^{(2)}=5\times10^{-3}$ (°)$^{-1}$, respectively. Their detection probabilities are $p_{\mathrm{D}}^{(1)}=p_{\mathrm{D}}^{(2)}=98\%$.

The AA fusion assigns the active and passive sensors with sensor weights $\alpha(1)=2/3$ and $\alpha(2)=1/3$. The average factors in the federated fusion are $\beta(0)=1/31$, $\beta(1)=20/31$, and $\beta(2)=10/31$. Other parameters are the same as in Section 5.1. The unscented transform (Hu GG et al., 2023) is employed to handle the nonlinearity resulting from Eqs. (47)–(49).

The active sensor's measurements (transformed into x and y coordinates), the passive sensor's bearings-only measurements, and the trajectory of the moving passive sensor are given in Fig. 10. The model probability error curves and the OSPA error curves of different algorithms are shown in Figs. 11 and 12.

As seen in Fig. 10, the passive sensor keeps tailgating motion via translations and rotations, as shown in Fig. 10a, so the mean of received bearings-only measurements in Fig. 10b is almost 0°. The three targets' bearings are intertwined, a common occurrence in reality. The target observability is satisfied, but its proof is not given as it is not our focus. In Figs. 11 and 12, the proposed federated fusion still yields the lowest model probability error and the lowest OSPA error. This result illustrates that our algorithm also exhibits its optimality in the designed heterogeneous fusion scenario despite the nonlinearity of the observation models in Eqs. (47)–(49).

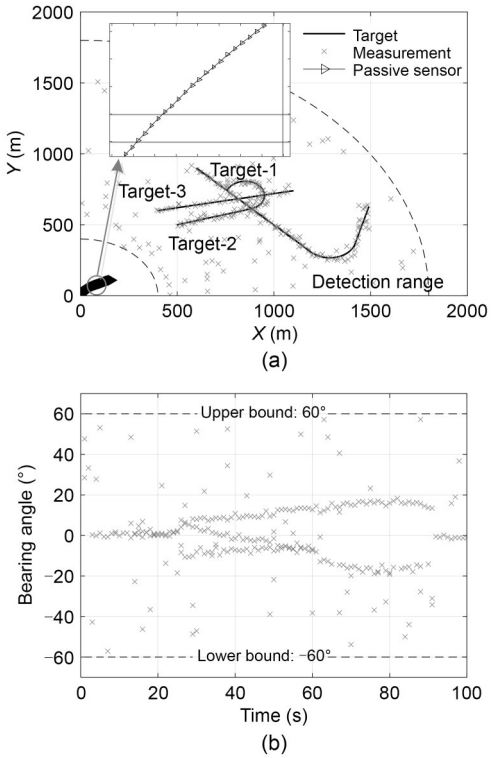

Fig. 10 Heterogeneous data: (a) active sensor's kinematic measurements; (b) passive sensor's bearings-only measurements

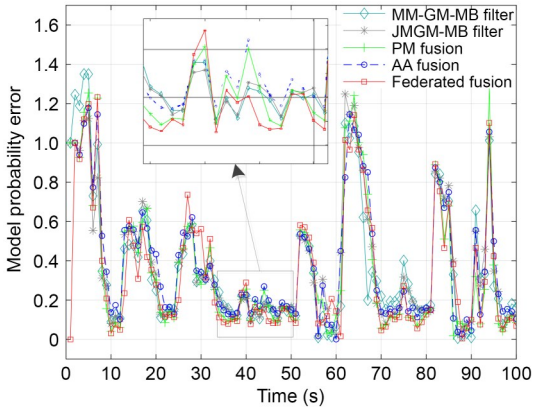

Fig. 11 Model probability error curves in heterogeneous fusion

5.5 Tolerance to missed detections

Finally, we test the proposed federated fusion's tolerance to missed detections.

We conduct 200 Monte Carlo runs of the AA fusion and the proposed federated fusion in the designed linear and heterogeneous scenarios with detection

probabilities $p_{\mathrm{D}}^{(s)}$=98%, 90%, 85%, 80%, and 70%. Figs. 13 and 14 present the box plots of OSPA errors in these two scenarios, the horizontal bars and lower/upper bounds of which reflect the median and min/max values, respectively, and the widths of which rely on the first and third quartiles.

As we can see, whether in the linear or the heterogeneous scenario, the centralized PM fusion exhibits significant vulnerability to missed detections, and the OSPA error of the proposed federated fusion is always lower than that of the AA fusion. Meanwhile, the federated fusion exhibits better tolerance to missed detections than the AA fusion: As the detection probability decreases (more frequent missed detections), our algorithm suffers less from performance reduction, which benefits from the master filter's ability to supplement missed detections. In contrast, the performance superiority of the federated fusion is more significant in the linear scenario. After all, the optimality in Section 3 is derived based on linear sensors. The centralized and decentralized fusion approaches of JMGM-MB filters, namely PM fusion and AA fusion, are summarized in supplementary materials.

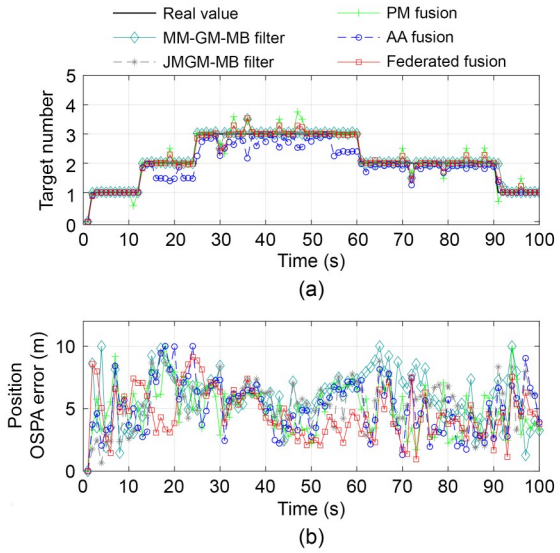

Fig. 12 Estimated target number (a) and OSPA error (b) curves

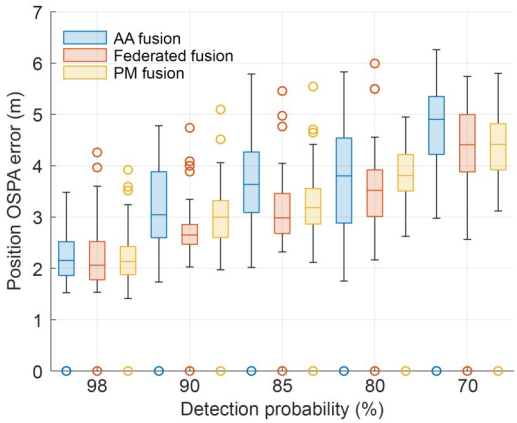

Fig. 13 Box plot in the linear scenario (References to color refer to the online version of this figure)

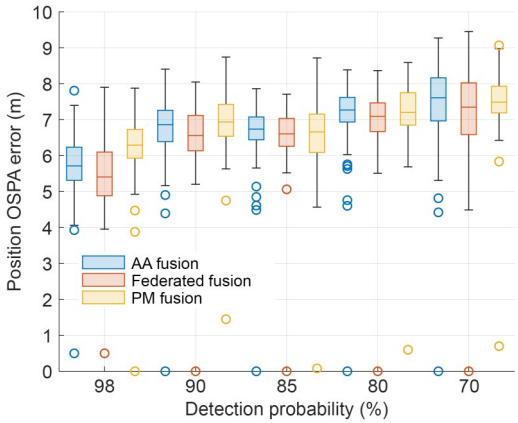

Fig. 14 Box plot in the heterogeneous scenario (References to color refer to the online version of this figure)

6 Conclusions

We propose a federated fusion algorithm of JMGM-MB filters to achieve optimal tracking of maneuvering targets in a hierarchical sensor network. This optimality is guaranteed by accurate association and the derived optimal fusion of single maneuvering targets. The former decomposes multi-target fusion into multiple single-target fusions, and the latter resorts to the covariance upper-bounding technique to eliminate correlations. A significant characteristic of the proposed algorithm is that a master filter is equipped to supplement missed detections, which is required by the optimal single-target fusion. Simulation results show that the proposed algorithm outperforms the centralized PM fusion and decentralized AA fusion in both linear and heterogeneous scenarios with any detection probability.

Due to the JMGM model's complexity, GA fusion has not been applied to aggregate JMGM-MB

filters. This is one of our future research directions. Another is to apply the JMGM model to implement other RFS filters, such as the PHD and CPHD filters.

Contributors

Yu XUE derived and implemented the proposed algorithm and drafted, revised, and finalized this paper. Xi'an FENG provided the resources needed and helped organize this paper.

Conflict of interest

Both authors declare that they have no conflict of interest.

Data availability

The data that support the findings of this study are available from the corresponding author upon reasonable request.

References

Balenzuela MP, Wills AG, Renton C, et al., 2022. Parameter estimation for jump Markov linear systems. *Automatica*, 135:109949. https://doi.org/10.1016/j.automatica.2021.109949

Carlson NA, 1990. Federated square root filter for decentralized parallel processors. *IEEE Trans Aerosp Electron Syst*, 26(3):517-525. https://doi.org/10.1109/7.106130

Chang CB, Athans M, 1978. State estimation for discrete systems with switching parameters. *IEEE Trans Aerosp Electron Syst*, AES-14(3):418-425. https://doi.org/10.1109/TAES.1978.308603

Da K, Li TC, Zhu YF, et al., 2020a. Gaussian mixture particle jump-Markov-CPHD fusion for multitarget tracking using sensors with limited views. *IEEE Trans Signal Inform Process Netw*, 6:605-616. https://doi.org/10.1109/TSIPN.2020.3016478

Da K, Li TC, Zhu YF, et al., 2020b. Kullback–Leibler averaging for multitarget density fusion. Proc 16th Int Symp on Distributed Computing and Artificial Intelligence, p.253-261. https://doi.org/10.1007/978-3-030-23887-2_29

Dong XD, Zhang XF, Zhao J, et al., 2021. Multi-maneuvering sources DOA tracking with improved interactive multi-model multi-Bernoulli filter for acoustic vector sensor (AVS) array. *IEEE Trans Veh Technol*, 70(8):7825-7838. https://doi.org/10.1109/TVT.2021.3093063

Dunne D, Kirubarajan T, 2013. Multiple model multi-Bernoulli filters for manoeuvering targets. *IEEE Trans Aerosp Electron Syst*, 49(4):2679-2692. https://doi.org/10.1109/TAES.2013.6621845

Gao L, Battistelli G, Chisci L, 2020. Multiobject fusion with minimum information loss. *IEEE Signal Process Lett*, 27: 201-205. https://doi.org/10.1109/LSP.2019.2963817

Georgescu R, Willett P, 2012. The multiple model CPHD tracker. *IEEE Trans Signal Process*, 60(4):1741-1751. https://doi.org/10.1109/TSP.2012.2183128

Gunay M, Orguner U, Demirekler M, 2016. Chernoff fusion of Gaussian mixtures based on sigma-point approximation. *IEEE Trans Aerosp Electron Syst*, 52(6):2732-2746. https://doi.org/10.1109/TAES.2016.150403

Hu GG, Xu LY, Gao BB, et al., 2023. Robust unscented Kalman filter-based decentralized multisensor information fusion for INS/GNSS/CNS integration in hypersonic vehicle navigation. *IEEE Trans Instrum Meas*, 72:8504011. https://doi.org/10.1109/TIM.2023.3281565

Hu XL, Zhang Q, Song BJ, et al., 2022. σ-threshold Bayes filter in unknown birth background with multi-Bernoulli finite sets. Proc IEEE Int Conf on Signal Processing, Communications and Computing, p.1-4. https://doi.org/10.1109/ICSPCC55723.2022.9984566

Julier SJ, Uhlmann JK, 1997. A non-divergent estimation algorithm in the presence of unknown correlations. Proc American Control Conf, p.2369-2373. https://doi.org/10.1109/ACC.1997.609105

Li GY, Battistelli G, Chisci L, et al., 2024. Distributed joint detection, tracking, and classification via labeled multi-Bernoulli filtering. *IEEE Trans Cybern*, 54(3):1429-1441. https://doi.org/10.1109/TCYB.2022.3208038

Li TC, 2024. Arithmetic average density fusion—part II: unified derivation for unlabeled and labeled RFS fusion. *IEEE Trans Aerosp Electron Syst*, 60(3):3255-3268. https://doi.org/10.1109/TAES.2024.3359592

Li TC, Corchado JM, Chen HM, 2018. Distributed flooding-then-clustering: a lazy networking approach for distributed multiple target tracking. Proc 21st Int Conf on Information Fusion, p.2415-2422. https://doi.org/10.23919/ICIF.2018.8455759

Li TC, Corchado JM, Sun SD, 2019a. Partial consensus and conservative fusion of Gaussian mixtures for distributed PHD fusion. *IEEE Trans Aerosp Electron Syst*, 55(5):2150-2163. https://doi.org/10.1109/TAES.2018.2882960

Li TC, Fan HQ, García J, et al., 2019b. Second-order statistics analysis and comparison between arithmetic and geometric average fusion: application to multi-sensor target tracking. *Inform Fus*, 51:233-243. https://doi.org/10.1016/j.inffus.2019.02.009

Li TC, Wang XX, Liang Y, et al., 2020. On arithmetic average fusion and its application for distributed multi-Bernoulli multitarget tracking. *IEEE Trans Signal Process*, 68:2883-2896. https://doi.org/10.1109/TSP.2020.2985643

Li TC, Song Y, Song EB, et al., 2024a. Arithmetic average density fusion—part I: some statistic and information-theoretic results. *Inform Fus*, 104:102199. https://doi.org/10.1016/j.inffus.2023.102199

Li TC, Yan RB, Da K, et al., 2024b. Arithmetic average density fusion—part III: heterogeneous unlabeled and labeled RFS filter fusion. *IEEE Trans Aerosp Electron Syst*, 60(1):1023-1034. https://doi.org/10.1109/TAES.2023.3334223

Li WL, Jia YM, 2011. Gaussian mixture PHD filter for jump Markov models based on best-fitting Gaussian approximation. *Signal Process*, 91(4):1036-1042.

https://doi.org/10.1016/j.sigpro.2010.08.004

Mahler R, 2014. Advances in Statistical Multisource-Multitarget Information Fusion. Artech House, Norwood, USA.

Ouyang C, Ji HB, Guo ZQ, 2012. Extensions of the SMC-PHD filters for jump Markov systems. *Signal Process*, 92(6):1422-1430. https://doi.org/10.1016/j.sigpro.2011.11.032

Peng C, Chai L, Yi W, et al., 2021. Distributed multi-sensor multi-view fusion of PHD filter for maneuvering targets. Proc CIE Int Conf on Radar, p.1182-1187. https://doi.org/10.1109/Radar53847.2021.10028507

Punithakumar K, Kirubarajan T, Sinha A, 2008. Multiple-model probability hypothesis density filter for tracking maneuvering targets. *IEEE Trans Aerosp Electron Syst*, 44(1): 87-98. https://doi.org/10.1109/TAES.2008.4516991

Schuhmacher D, Vo BT, Vo BN, 2008. A consistent metric for performance evaluation of multi-object filters. *IEEE Trans Signal Process*, 56(8):3447-3457. https://doi.org/10.1109/TSP.2008.920469

Shen-Tu H, Lin RF, Shen WC, et al., 2024. An arithmetic geometric mixed average GM-PHD algorithm for decentralized sensor network with limited field of view. *IEEE Sens J*, 24(12):19995-20008. https://doi.org/10.1109/JSEN.2024.3392891

Sun SL, 2020. Distributed optimal linear fusion estimators. *Inform Fus*, 63:56-73. https://doi.org/10.1016/j.inffus.2020.05.006

Sun YC, Kim D, Hwang I, 2022. Multiple-model Gaussian mixture probability hypothesis density filter based on jump Markov system with state-dependent probabilities. *IET Radar Sonar Navig*, 16(11):1881-1894. https://doi.org/10.1049/rsn2.12304

Üney M, Clark DE, Julier SJ, 2013. Distributed fusion of PHD filters via exponential mixture densities. *IEEE J Sel Top Signal Process*, 7(3):521-531. https://doi.org/10.1109/JSTSP.2013.2257162

Üney M, Houssineau J, Delande E, et al., 2019. Fusion of finite-set distributions: pointwise consistency and global cardinality. *IEEE Trans Aerosp Electron Syst*, 55(6):2759-2773. https://doi.org/10.1109/TAES.2019.2893083

Vo BT, Vo BN, Cantoni A, 2009. The cardinality balanced multi-target multi-Bernoulli filter and its implementations. *IEEE Trans Signal Process*, 57(2):409-423. https://doi.org/10.1109/TSP.2008.2007924

Wang KW, Zhang Q, Hu XL, 2024. Multisensor multitarget tracking arithmetic average fusion method based on probabilistic time window. *IEEE Sens J*, 24(3):3583-3593. https://doi.org/10.1109/JSEN.2023.3337267

Wei JX, Luo F, Chen SC, et al., 2023. Robust fusion of GM-PHD filters based on geometric average. *Signal Process*, 206:108912. https://doi.org/10.1016/j.sigpro.2022.108912

Wu SY, Dong XD, Zhao J, et al., 2019. A fast implementation of interactive-model generalized labeled multi-Bernoulli filter for interval measurements. *Signal Process*, 164:345-353. https://doi.org/10.1016/j.sigpro.2019.05.028

Wu WH, Cai YC, Jin HB, et al., 2021a. Derivation of the multi-model generalized labeled multi-Bernoulli filter: a solution to multi-target hybrid systems. *Front Inform Technol Electron Eng*, 22(1):79-87. https://doi.org/10.1631/FITEE.2000105

Wu WH, Sun HM, Huang ZL, et al., 2021b. Multi-GMTI fusion for Doppler blind zone suppression using PHD fusion. *Signal Process*, 183:108024. https://doi.org/10.1016/j.sigpro.2021.108024

Xie X, Sun HM, Wu WH, et al., 2019. Multi-UAV multi-target tracking in the presence of Doppler blind zone. Proc IEEE Int Conf on Unmanned Systems, p.438-442. https://doi.org/10.1109/ICUS48101.2019.8996083

Xie XX, Wang Y, Guo JQ, et al., 2023. The multiple model Poisson multi-Bernoulli mixture filter for extended target tracking. *IEEE Sens J*, 23(13):14304-14314. https://doi.org/10.1109/JSEN.2023.3270272

Xue Y, Feng XA, 2024. Joint multi-Gaussian mixture model and its application to multi-model multi-Bernoulli filter. *Dig Signal Process*, 153:104616. https://doi.org/10.1016/j.dsp.2024.104616

Yang H, Li TC, Yan JK, et al., 2024. Hierarchical average fusion with GM-PHD filters against FDI and DoS attacks. *IEEE Signal Process Lett*, 31:934-938. https://doi.org/10.1109/LSP.2024.3356823

Yi W, Li SQ, Wang BL, et al., 2020. Computationally efficient distributed multi-sensor fusion with multi-Bernoulli filter. *IEEE Trans Signal Process*, 68:241-256. https://doi.org/10.1109/TSP.2019.2957638

Zhao BF, 2024. Multisensor maneuvering target fusion tracking using interacting multiple model. *Autom Contr Comput Sci*, 58(3):303-312. https://doi.org/10.3103/S0146411624700184

Zhou YQ, Yan LP, Li H, et al., 2024. The multiple pairwise Markov chain model-based labeled multi-Bernoulli filter. *J Franklin Inst*, 361(10):106939. https://doi.org/10.1016/j.jfranklin.2024.106939

List of supplementary materials

1 Covariance upper-bounding technique
2 Graphical summary of conditional merging
3 Sequential fusion of IMM filters and its simulation
4 Centralized PM fusion of JMGM-MB filters
5 Decentralized AA fusion of JMGM-MB filters